# Localized and Delocalized Motion of Colloidal Particles on a Magnetic Bubble Lattice

Pietro Tierno,[1] Tom H. Johansen,[2] and Thomas M. Fischer[1,*]

[1]*Department of Chemistry and Biochemistry, Florida State University, Tallahassee, Florida, USA*
[2]*Department of Physics, University of Oslo, Blindern, Norway*

(Received 28 March 2007; published 20 July 2007)

We study the motion of paramagnetic colloidal particles placed above magnetic bubble domains of a uniaxial garnet film and driven through the lattice by external magnetic field modulation. An external tunable precessing field propels the particles either in localized orbits around the bubbles or in superdiffusive or ballistic motion through the bubble array. This motion results from the interplay between the driving rotating signal, the viscous drag force and the periodic magnetic energy landscape. We explain the transition in terms of the incommensurability between the transit frequency of the particle through a unit cell and the modulation frequency. Ballistic motion dynamically breaks the symmetry of the array and the phase locked particles follow one of the six crystal directions.

DOI: 10.1103/PhysRevLett.99.038303 PACS numbers: 82.70.Dd, 66.20.+d, 67.40.Hf

A particle driven through a periodic potential with pinning sites reveals fascinating dynamics which encompass localization at the pinning sites, ballistic motion through the lattice, or even superdiffusive (chaotic) motion. Theoretical models cover a broad range of phenomena, e.g., atomic diffusion on metallic surfaces [1], flux flow in Josephson-junction arrays [2], and the motion of phonons in the Frenkel-Kontorova model [3]. Recent experiments with holographic optical tweezer [4,5], have shown that colloidal particles represent an experimentally accessible model system to investigate how the particle dynamics is affected by a corrugated potential. There, a periodic potential was generated with a laser using diffractive elements. However there is a rich variety of means to achieve miniaturized periodic patterns resulting in, e.g., high dielectric or magnetic susceptibility contrast modulations. In particular, cylindrical magnetic ''bubble'' domains in uniaxial garnet films provide strong and externally tunable magnetic pinning sites at the location of the domain walls of the magnetic bubbles. External modulations alter the bubble domain pattern and drive paramagnetic particles placed above the film through the bubble array.

The ability to tune the particle interaction with the pinning lattice and to vary the strength or frequency of the external driving modulation leads to novel implications for both device fabrication [6] and fundamental studies [7].

Here we report on the externally driven dynamics of paramagnetic colloidal particles in an aqueous solution above a regular lattice of magnetic bubbles. A precessing external magnetic field simultaneously controls the bubble array pattern and the colloidal particle motion. The field precession lets the colloidal particles either orbit around one localized magnetic bubble, stochastically or ballistically move through the bubble lattice, or confines the motion to the interstitial region between the neighboring bubbles. We show that the different regimes of motion are controlled by the precession frequency $\Omega$, and the normal component of the magnetic field $H_z$. Using video microscopy with a particle tracking routine, we identify the transitions between the various regimes and determine the full dynamical phase diagram of the driven system.

To create a magnetic bubble lattice we use a ferrite garnet film with uniaxial anisotropy and composition $Y_{2.5}Bi_{0.5}Fe_{5-q}Ga_qO_{12}$ ($q = 0.5$–1), thickness $\sim 5\ \mu$m and saturation magnetization $M_s = 1.7 \times 10^4$ A/m. The equilibrium domain pattern of such a film is a stripe labyrinth pattern. High frequency ($\sim 12 \times 10^3\ s^{-1}$) magnetic field pulses of amplitude $\sim 10^5$ A/m normal to the film enforce the formation of the metastable magnetic bubbles inside the garnet film. The bubbles are cylindrical domains, with diameter $2R = 8.2 \pm 0.1\ \mu$m, of reverse magnetization separated by a continuous magnetized film (see Fig. 1) [8]. Application of an external magnetic field $H_z$ parallel (antiparallel) to the bubble magnetization direction increases (decreases) the size of the cylindrical domains. For the magnetic field strengths used here, $H_z <$ 7000 A/m, the bubble shape remains circular and the lattice keeps its hexagonal form, as seen from the microscope images in Fig. 1. The bubble array pattern is then fully described by the lattice constant $a$ and the bubble area fraction $\Phi$ [9]. In part (b) of Fig. 1 we show the continuous domain area fraction $1 - \Phi$ (squares) and the lattice constant $a$ (circles) of the lattice measured as a function of the external magnetic field. The bubble area fraction linearly decreases with increasing magnetic field $H_z$ normal to the film while the lattice constant only changes marginally [10].

The colloidal suspension consist of polystyrene paramagnetic particles with a diameter $D = 2.8\ \mu$m and effective magnetic susceptibility $\chi = 0.17$ (Dynabeads M-270). In aqueous solution the particles are electrostatic stabilized by the dissociation of surface carboxylic groups ($COO^-$). We coat the film with a thin layer of polysodium-4-styrene sulfonate to prevent adhesion of the particles to the film [11]. A water drop containing $\sim 7 \times 10^6$ beads/ml was placed on top of the garnet film and the particle

 

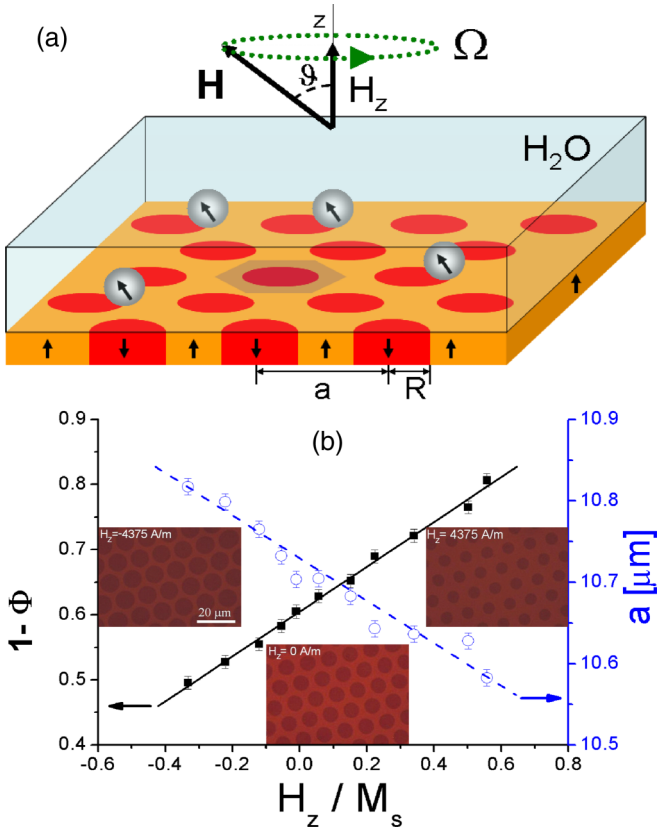


FIG. 1 (color online). (a) Scheme showing a magnetic bubble lattice [radius $R$, lattice constant $a$, one unit cell is shaded in blue (gray)] with paramagnetic particles deposited on top of it. The magnetic field $\mathbf{H}$ precesses with frequency $\Omega$ under an angle $\vartheta$ around the $z$ axis. (b) Continuous domain area fraction $1-\Phi$ (filled squares) and lattice constant (open circles) for a bubble array at different values of the $z$ component of the field, $H_z$. The insets show polarization microscopy images of the film at different fields $H_z$.

sediment without adhering to the polymer coating [see Fig. 1(a)]. Three coils perpendicular to each other provide the external magnetic field. The video-microscope used to visualize the particles and the magnetic bubble array has been described in detail in Ref. [12].

In a magnetic field $\mathbf{H}$ a paramagnetic particle of volume $V$ acquires a magnetic moment $\mathbf{m} = V\chi\mathbf{H}$ along the field. Its magnetic energy is $E = -\mu\mathbf{m}\cdot\mathbf{H} \propto H^2$, where $\mu$ is the magnetic susceptibility of the water. Without external field, the particles are attracted toward the bubble domain walls, where the magnetic stray field of the film is maximal. If we ignore the field of the neighboring magnetic bubbles the field has cylindrical symmetry and each particle position on the bubble domain boundary has the same energy. One can break this symmetry with an external field. We use a precessing magnetic field of frequency $\Omega$ and precession angle $\vartheta$:

$$\mathbf{H} = \hat{H}[\cos\vartheta\mathbf{e}_z + \sin\vartheta(\cos(\Omega t)\mathbf{e}_x + \sin(\Omega t)\mathbf{e}_y)]. \quad (1)$$

This field, when averaged over one period of the modulation, has no preferred direction and motion into a particular direction can only be achieved via symmetry breaking for the individual particles. The macroscopic particle flux vanishes identically since the dipole interaction between the particles are negligible compared to the particle garnet film interaction. We independently vary the normal component of the external field, $H_z = \hat{H}\cos\vartheta$ which alters the size of the bubble domains, and the frequency of the rotating in-plane component $H_{xy}$ that modulates the periodic energy landscape in time. The planar magnetic field component $H_{xy}$ is small ($H_{xy} < 10^4$ A/m) and does not deform the magnetic bubble array. However, it allows us to change the magnetic energy landscape *above* the garnet film.

Diffusion and transport of a colloidal particle can be characterized by the correlation function

$$C(\tau) = \langle(\mathbf{r}(t) - \mathbf{r}(t+\tau))^2\rangle \sim \tau^{\alpha}, \quad (2)$$

with $\mathbf{r}(t)$ the two-dimensional particle position at time $t$ and $\langle\cdots\rangle$ a time average. In the present experiment we find in the long time limit a power law behavior with exponent $\alpha$. Depending on the field and frequency we observe localized ($\alpha = 0$), superdiffusive ($\alpha > 1$), and ballistic ($\alpha = 2$) motion of the particles.

First, we show the effect of varying the magnetic field $H_z$ normal to the film at constant frequency and constant in-plane magnetic field component ($\Omega = 21.9$ s$^{-1}$, $H_{xy} = 1432$ A/m). Figure 2 shows the correlation function versus time for a particle in the driven system at four different values of $H_z$. Periodic behavior of $C(\tau)$ was found for both small fields, $H_z < 0.21 M_s$ and for sufficiently large fields,

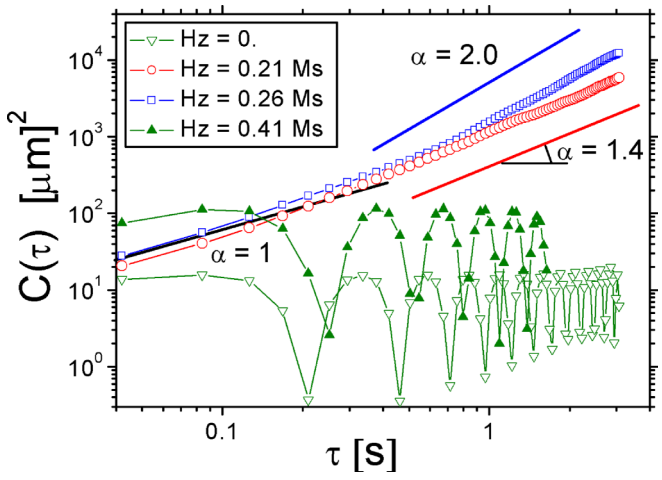


FIG. 2 (color online). Correlation function versus time for different values of the normal field $H_z$ ($\Omega = 21.9$ s$^{-1}$, $H_{xy} = 1432$ A/m). The continuous line shows a power law fit for the ballistic (open squares) and superdiffusive (open circles) behavior. The green (gray) lines correspond to $C(\tau)$ for the localized state obtained at low (open triangle) and high (closed triangles) field strength.

$H_z > 0.36M_s$, as exemplified by the graphs for $H_z = 0$ (open triangles) and $H_z = 0.41M_s$ (filled triangles), respectively. These field intervals represent two different regimes of localized particle motion. At low fields, the particles are orbiting along the circular bubble boundary [13]. Increasing $H_z$ decreases the bubble size and increases the interstitial region between adjacent bubbles. At the threshold value $H_z^1 = 0.21M_s$, the particle orbit around the bubble becomes unstable and the particle starts to move through the lattice on top of the continuous domain by orbiting around roughly half of a magnetic bubble before moving on to the next bubble. Near the threshold, this delocalized motion is characterized by a superdiffusive exponent of $\alpha = 1.4$. The exponent $\alpha$ continuously increases with $H_z$ ($0.21M_s \leq H_z \leq 0.24M_s$) and the typical particle trajectory straightens out with increasing persistence length of the path. Eventually the exponent $\alpha$ levels off close to $\alpha = 2$ and we observe a ballistic motion of the particle through the bubble array. This dynamical region extend up to a field of $0.34M_s$. Further increase of $H_z$ induces dynamic transitions in reversed order. The system returns to a superdiffusive behavior in the range $0.34M_s \leq H_z \leq 0.36M_s$. Above, $H_z > 0.36M_s$, the particle becomes again localized and now with a triangular orbit around the interstitial region between three magnetic bubbles [bottom (d) of Fig. 3]. Typical particle trajectories in the various regimes are depicted in the bottom of Fig. 3 and in videos in [14].

Shown in the upper panel of Fig. 3 is the full phase diagram of the motion as a function of $H_z$ and $\Omega$ and the variation of the exponent $\alpha$ with $H_z$ is shown for $\Omega = 21.9\ \mathrm{s}^{-1}$ in the inset. The diagram underscores that the transition from a localized orbit toward a ballistic motion via the intermediate superdiffusive regime is a common feature of this transition. All thresholds in $H_z$ increase with increasing frequency $\Omega$ up to $\Omega = 60\ \mathrm{s}^{-1}$. At this frequency the different thresholds start to approach each other and above $\Omega = 123\ \mathrm{s}^{-1}$ the ballistic motion is no longer possible. At frequencies exceeding $\Omega = 160\ \mathrm{s}^{-1}$ also the superdiffusive regime vanishes and the particles are localized for all values of $H_z$.

The presence of the two superdiffusive regions bridging the localized and ballistic motion suggests a continuous transition from one dynamical state to the next one.

At low $H_z$ the particles are localized and orbit the bubbles. The field $H_z$ displaces the particles from the bubble boundaries into the continuous domain leading to orbits with larger radius as the $H_z$ increases while the bubble radius itself decreases. Obviously the trapping efficiency of a bubble decreases with increasing $H_z$. The particles orbit the bubbles with a frequency $\omega_o = \Omega$ that is synchronous with the external field frequency in the entire localized regime. As soon as the motion enters the superdiffusive regime there is no longer an orbit frequency around the bubble. Instead we characterize the motion by

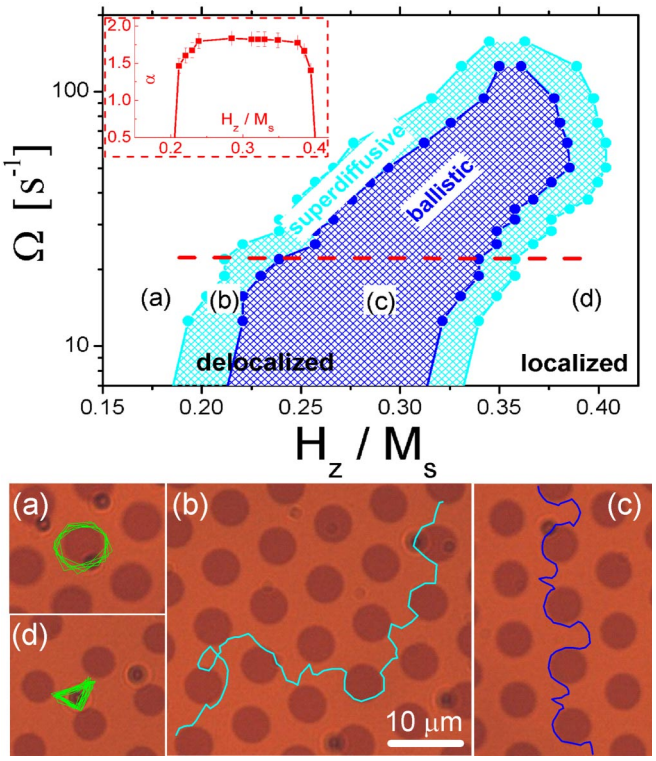


FIG. 3 (color online). Phase diagram of the exponent $\alpha$ in the $(H_z/M_s, \Omega)$ plane. White region denote localize colloidal state, cyan (gray) superdiffusive motion and blue (black) ballistic motion. The inset shows the behavior of $\alpha$ with $H_z$ along the red (gray) cut in the phase diagram. Particle trajectory of the localized [(a),(d) in green-white] and delocalized states [(b),(c) in gray] are superimposed on the images on the bottom.

the transit frequency $\omega_t = 2\pi/T$ of a particle traversing one unit cell of the bubble array, where $T$ is the transit time averaged over the total path of the superdiffusive particle. Figure 4 shows the behavior of $\omega_o$ and $\omega_t$ versus $H_z$. We find that the superdiffusive regime has a transit frequency that is incommensurable to the modulation frequency. The particles need more than a cycle to traverse one unit cell. If the transition from localized to superdiffusive motion is of second order one would expect the normalized transit frequency $\omega_t/\Omega$ to increase continuously from zero as one enters the superdiffusive regime. In Fig. 4 we see an increase in $\omega_t$ versus $H_z$. However, whether or not this frequency rises from zero upon entering the superdiffusive regime cannot be resolved with our measurements. In the ballistic regime the transit frequency $\omega_t$ becomes synchronized with the modulation frequency. The ballistic path of the trajectory of Fig. 3(c) is not entirely periodic. When the particles leave one bubble and move to the next they meander slightly in the region between the bubbles. The time spent between the bubbles is used to restore the phase locking with the external signal. The particles have some time to rest in the interstitial region waiting there to be picked up by the energy minimum circling around the next

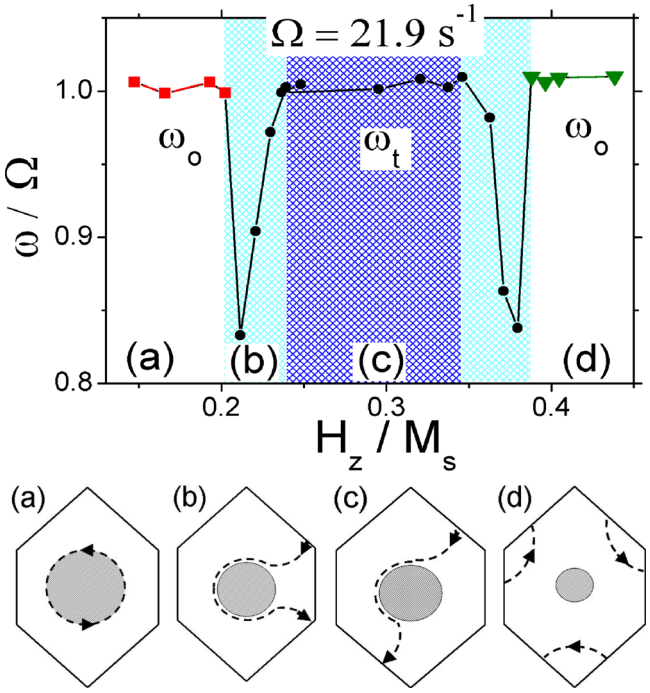


FIG. 4 (color online). Orbit and transit frequency through the unit cell as a function of the normal field $H_z$. The squares and triangles are for orbital frequency, $\omega_o$, the circles for frequency of transit $\omega_t$. On the bottom line are schematics (a)–(d) that show the corresponding particle trajectory.

bubble. The rest in the interstitial region hence serves as a feedback mechanism correcting for possible errors in phase during the motion from one unit cell to the next.

It should also be emphasized that the ballistic regime is not a result of some preferred direction. We observe particles moving in any of the six crystallographic directions of the array. The direction of motion is decided by the phase of the particle. Particles traveling in directions $\phi = n2\pi/6$ have a corresponding phase lag and move from one bubble to the next at times $t = nT/6$. A movie (ballistic2.mpg) of particles simultaneously moving in different crystallographic directions is available as supporting information in [14]. When we increase $H_z$ to enter the second superdiffusive regime the transition frequency $\omega_t$ drops again and becomes incommensurate to the modulation frequency. Also the role of the interstitial and the bubble domain regions becomes reversed. Particles are now more attracted to the interstitial region and repelled from the bubble boundaries, there orientation is dominated by $H_z$ that is oriented antiparallel to the bubbles. At large values of $H_z$ the particles become localized and orbit the interstitials. In the bottom of Fig. 4 we summarize the various modes of motion by showing typical trajectories of the particles through the unit cell.

In conclusion, we have shown experimentally a novel system with emergent phenomena such as ballistic [15] and superdiffusive [16] transport of particles through a periodic energy landscape. In contrast to recent numerical predictions [15] no external field that breaks the sixfold symmetry is needed to obtain a ballistic transport in one of the symmetry broken ballistic directions. We explored the dynamics of paramagnetic colloidal particles driven through a magnetic bubble lattice by external magnetic field modulation. We observe a sequence of field induced transitions from localized motion via superdiffusive transport to a ballistic motion and reverse. Measurement of the transit frequency through a unit cell reveals an incommensurability of the transit and modulation frequency in the superdiffusive regime. The emerging motion may be useful for microfluidic applications like the programmed directed or dispersed transport of biological entities attached to the colloidal particles.

T. H. J. thanks The Research Council of Norway for financial support.

*tfischer@chem.fsu.edu

[1] J. W. M. Frenken and B. J. Hinch, *Helium Atom Scattering from Surfaces* (Springer-Verlag, New York, 1992).
[2] C. Reichhardt and F. Nori, Phys. Rev. Lett. **82**, 414 (1999).
[3] Bambi Hu, L. Yang, and Y. Zhang, Phys. Rev. Lett. **97**, 124302 (2006).
[4] P. T. Korda, M. B. Taylor, and D. G. Grier, Phys. Rev. Lett. **89**, 128301 (2002).
[5] K. Mangold, P. Leiderer, and C. Bechinger, Phys. Rev. Lett. **90**, 158302 (2003).
[6] W. D. Volkmuth and R. H. Austin, Nature (London) **358**, 600 (1992).
[7] J. P. Gleeson, J. M. Sancho, A. M. Lacasta, and K. Lindenberg, Phys. Rev. E **73**, 041102 (2006).
[8] K. L. Babcock and R. M. Westervelt, Phys. Rev. A **40**, 2022 (1989).
[9] S. Wurlitzer, T. M. Fischer, and H. Schmiedel, J. Chem. Phys. **116**, 10877 (2002).
[10] A. A. Thiele, Bell Syst. Tech. J. **48**, 3287 (1969).
[11] L. E. Helseth, H. Z. Wen, T. M. Fischer, and T. H. Johansen, Phys. Rev. E **68**, 011402 (2003).
[12] P. Tierno, R. Muruganathan, and T. M. Fischer, Phys. Rev. Lett. **98**, 028301 (2007).
[13] P. Tierno, T. H. Johansen, and T. M. Fischer, J. Phys. Chem. B **111**, 3077 (2007).
[14] See EPAPS Document No. E-PRLTAO-99-004729 for movies of the motion of the particles. For more information on EPAPS, see http://www.aip.org/pubservs/epaps.html.
[15] C. Reichhardt, C. J. Olson, and M. B. Hastings, Phys. Rev. Lett. **89**, 024101 (2002).
[16] J. D. Bao, Y. Zhou, and K. Lu, Phys. Rev. E **74**, 041125 (2006).